Available online at www.sciencedirect.com
SCIENCE DIRECT®
Biomaterials 25 (2004) 5405–5413
Biomaterials
www.elsevier.com/locate/biomaterials

Cell response to dextran-derivatised iron oxide nanoparticles post internalisation

Catherine Cecilia Berry*, Stephen Wells, Stuart Charles, Gregor Aitchison, Adam S.G. Curtis

Centre for Cell Engineering, University of Glasgow, Joseph Black Building, IBLS University Avenue, Glasgow G12 8QQ, UK

Received 25 July 2003; accepted 19 December 2003

Abstract

Magnetic nanoparticles have been used for many years as magnetic resonance imaging contrast agents. Despite the fact that there are currently several dextran-coated iron oxide nanoparticles are in preclinical and clinical use, there is very little information available concerning the influence such particles have on cells in culture. The prerequisite for particles employed as contrast agents is capture and subsequent uptake by cells. This study involved the use of magnetic nanoparticles synthesised and derivatised with dextran, compared to similar underivatised plain particles. The influence in vitro was assessed using human dermal fibroblasts and various techniques to observe cell–particles interaction, including light and fluorescence microscopy, scanning and transmission electron microscopy. The results indicate that although both the uncoated and the dextran-derivatised particles are uptaken into the cell, the derivatised particles induce alterations in cell behaviour and morphology distinct from the plain particles, suggesting that cell response is dependent on the particles coating.

Keywords: Nanoparticle; Magnetism; Dextran; In vitro test; Cell viability; Cell culture; Fluorescence

1. Introduction

Cell labelling with magnetic nanoparticles is an increasingly common method for in vitro cell separation as well as for in vivo imaging owing to their enhancing signal properties in magnetic resonance imaging (MRI) [1–3]. In addition, there are promising advances in magnetic intracellular hyperthermia [4–6]. To date a wide variety of magnetic nanoparticles have been produced, differing in size (hydrodynamic particle size varying from 10 to 500 nm) [7] and type of coating material used, such as dextran, starch, albumin, silicones and poly(ethyleneglycol) (PEG) [8,9]. Dextran has proved to be one of the most common coatings utilised, as they have proven to be long circulating with no measurable reported toxicity index LD_{50} [10,11] and as a result, some preparations are currently being used in clinical trials [12]. Dextran derivitised nanoparticles are classified into two main groups according to their size, as this affects plasma half-life and biodistribution [13].

Biologically speaking, the main requirement for MRI is that the cells efficiently capture the magnetic particles they are exposed to, and subsequently internalise them. Most current labelling techniques use one of two approaches: (1) attaching magnetic nanoparticles to the cell surface or (2) internalising the nanoparticles by fluid phase endocytosis, receptor mediated endocytosis or phagocytosis [14–16]. The endocytotic process can be broken down into several main steps that include membrane invagination, clathrin coated pit formation, detachment of the newly formed vesicle via action of the small GTPase dynamin and finally movement of this new endocytic compartment away from the plasma membrane into the cytosol [17].

Previous studies have reported cellular uptake of dextran-coated nanoparticles varying from 0.011 to 0.118 pg of iron per cell (1 h incubation at 37°C) in various tumour cells and a maximum load of 0.97 pg in primary isolated peritoneal mouse macrophages [11,18,19]. If a cell can be sufficiently loaded with

*Corresponding author. Tel.: +44-141-3303550; fax: +44-141-3303730.
E-mail address: catherine.berry@bio.gla.ac.uk (C.C. Berry).

0142-9612/$ - see front matter © 2003 Elsevier Ltd. All rights reserved.
doi:10.1016/j.biomaterials.2003.12.046

magnetic material, then MRI can also be adopted for use in cell tracking, as it can have a resolution of 20–25 μm, approaching the size of a single cell [20].

There is very little information in the literature, however, concerning the effect of such loading on cell behaviour, with most studies only concerned with the fate of the particles with regards uptake after several hours incubation [1,18]. This paper therefore aims to investigate the influence of such dextran derivatised (DD) magnetic nanoparticles on cells in vitro for up to 48 h, well after particle internalisation should have occurred. The iron oxide nanoparticles (8–15 nm) were synthesised and derivatised with dextran, producing stable fluids of neutral pH. The influence in vitro was assessed, and compared to underivatised particles, in terms of cell viability/apoptosis, cell morphology, particle uptake, observation of cytoskeleton (F-actin and tubulin), rac and clathrin localisation, and cell motility.

The findings show that the underivatised particles appeared to be largely internalised by the fibroblasts, contributing to eventual cell death, possibly through apoptotic means. The DD particles followed a similar fate with regards uptake and possible cell death, a surprising response given the literature regarding LD_{50} indexes. There were also several changes evident in cell behaviour, particularly with cell morphology/cytoskeletal organisation and cell motility. Such findings indicate the importance of understanding nanoparticle–cell interactions prior to use in in vivo situations.

2. Materials and methods

2.1. Nanoparticle synthesis

Magnetite nanoparticles of approximately 10 nm diameter were precipitated in alkali solution from solutions of Fe(II) and Fe(III) chloride according to the standard co-precipitation technique of Reimers and Khalafalla [21].

Magnetite nanoparticles of approximately 8 nm diameter stabilised with dextran in water were prepared in situ by co-precipitation from an iron salt–dextran solution. This method was based on the work of Molday and McKenzie [22]. Immediately following dextran stabilisation, samples were dialysed against deionised water using MWCO 50 000 dialysis tubing for 4–5 days, with water changes twice daily, with constant monitoring of the conductivity until it falls below 10 μS/cm.

2.2. Nanoparticle size determination

The average particle size and distribution were determined using two individual methods. Initial observations were done via transmission electron microscopy (TEM, Zeiss 902, voltage −80 kV). The aqueous dispersion of the particles was drop cast onto a carbon coated copper grid, which was subsequently air dried at room temperature before loading into the microscope.

Additionally, the nanoparticle size, and magnetic properties, were assessed using a vibrating sample magnetometer (LRL) on liquid samples.

2.3. Cell culture

Infinity™ Telomerase Immortalised primary human fibroblasts (hTERT-BJ1, Clonetech Laboratories, Inc. USA) were seeded onto glass coverslips (13 mm diameter) at a density of 1×10^4 cells per disk in 1 ml of complete medium. The medium used was 71% Dulbeccos Modified Eagles Medium (DMEM) (Sigma, UK), 17.5% Medium 199 (Sigma, UK), 9% foetal calf serum (FCS) (Life Technologies, UK), 1.6% 200 mM L-glutamine (Life Technologies, UK) and 0.9% 100 mM sodium pyruvate (Life Technologies, UK). The cells were incubated at 37°C with a 5% CO_2 atmosphere for 24 h. At this time point the cells were incubated in complete medium supplemented with 0.05 mg ml^{-1} DD and underivatised plain (P) nanoparticles for a further 24–48 h. All control cells were cultured in the absence of any particles.

2.4. Cell viability/apoptosis

An annenin V detection kit (Sigma) was employed to assess cell viability and apoptosis. The kit comprised of two individual stains; the binding of annexin V dye (AnnCy3—red fluorescence) to phosphatidylserine present in the outer membrane of cells that are starting the apoptotic process [23] and 6-carboxyfluorescein diacetate (6-CFDA—green fluorescence) to assess cell viability. This allowed differentiation between apoptotic and necrotic cells (apoptotic appearing yellow). After 48 h of incubation with the nanoparticles, the cells were washed in the kit binding buffer prior to being incubated in both AnnCy3 and 6-CFDA (diluted as directed in buffer) for 10 min at room temperature. Samples were then washed in buffer and immediately viewed by fluorescence microscopy (Vickers M17) with images captured using a Hamamatsu Argus 20. In addition, apoptosis was induced with prior incubation in staurosporin as a positive control [24,25]. The total number of apoptotic cells in each cell population were counted and expressed graphically.

2.5. Scanning electron microscopy (SEM) of cell morphology

The cells were fixed with 1.5% gluteraldehyde (Sigma, UK) buffered in 0.1 M sodium cacodylate (Agar, UK)

(4°C, 1 h) after a 24 h incubation in the nanoparticles. The cells were then post-fixed in 1% osmium tetroxide for 1 h (Agar, UK) and 1% tannic acid (Agar, UK) was used as a mordanant. Samples were dehydrated through a series of alcohol concentrations (20%, 30%, 40%, 50%, 60%, 70%), stained in 0.5% uranyl acetate, followed by further dehydration (90%, 96%, 100% alcohol). The final dehydration was in hexamethyldisilazane (Sigma, UK), followed by air-drying. Once dry, the samples were coated with gold before examination with a Hitachi S800 field emission SEM at an accelerating voltage of 10 keV.

2.6. Fluorescent cytoskeletal observation and rac localisation

After 24 h culture with the nanoparticles, cells were fixed in 4% formaldehyde/PBS, with 1% sucrose at 37°C for 15 min. The samples were then washed with PBS, and permeabilising buffer was added at 4°C for 5 min. The samples were then incubated at 37°C for 5 min in 1% BSA/PBS. This was followed by the addition of either anti-β-tubulin or anti-rac primary antibody (1:100 in 1% BSA/PBS, monoclonal anti-human raised in mouse (IgG1), Sigma, Poole, UK) for 1 h (37°C). Simultaneously, rhodamine conjugated phalloidin was added for the duration of this incubation (1:100 in 1% BSA/PBS, Molecular Probes, Oregon, USA). The samples were then washed in 0.5% Tween 20/PBS and a secondary, biotin conjugated antibody, (1:50 in 1% BSA/PBS, monoclonal horse anti-mouse (IgG), Vector Laboratories, UK) was added for 1 h (37°C) followed by more washing. A FITC conjugated streptavidin third layer was added (1:50 in 1% BSA/PBS, Vector Laboratories, UK) at 4°C for 30 min, and given a final wash. Samples were then viewed by fluorescence microscope (Vickers M17) with images captured using a Hamamatsu Argus 20.

2.7. Quantification of fluorescently labelled particle uptake

Particle uptake was verified by fluorescently coating the nanoparticles followed by observation using fluorescence microscopy. The method was adapted from a technical immunology book [26]. Briefly, both P and DD nanoparticles were dialysed against 0.15 M sodium chloride (3 changes of solution over 2 days), followed by dialysis against 0.05 M bicarbonate buffered saline (BBS, pH 8.5) for 5 h and a final dialysis against 0.05 M BBS (pH 9.2) for 2 h. The particles were then dialysed against 100 μg of the fluorochrome fluorescein-5-isothiocyanate (FITC, Molecular Probes) in 0.05 M BBS (pH 9.2) for a further 14–16 h (with the volume of the 'chrome exactly 10 times that of the sample). Finally, the above reaction was halted by dialysis against 0.02 M phosphate buffered saline (PBS, pH 7.0) for 2–3 h. Note that all dialysis was performed at 4°C.

Cells were subsequently incubated in the particles for 2 h and samples viewed by fluorescence microscope (Vickers M17) with images captured using a Hamamatsu Argus 20. For quantification of particle uptake an in-house method was then used that relied on ImageJ imaging software downloaded from the National Institute of Health (USA) (NIH Image-free download available at http://rsb.info.nih.gov/nih-image). This used automated detection of the intensity of stain per image, with five cells counted for four replicates (note that standardised illumination conditions were used throughout). Student's t-test (for two samples assuming unequal varience) was used to compare statistical significance of the control cells with those incubated in P and DD nanoparticles (differences: $^{*}p \leqslant 0.05$).

2.8. Clathrin immunofluorescence

After 24 h culture with the nanoparticles, cells were treated exactly as for cytoskeletal observation, the only variation being that an anti-clathrin (1:50 in 1% BSA/PBS, monoclonal anti-human raised in mouse, Biogenesis, UK) primary antibody was used in the initial incubation. Samples were then viewed by fluorescence

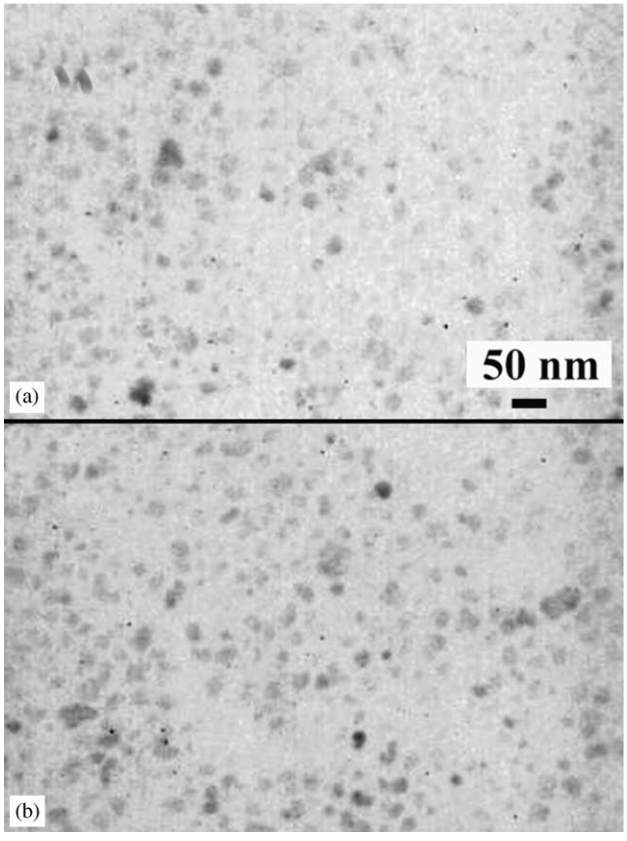

Fig. 1. TEM Image of (a) P particles and (b) DD particles.

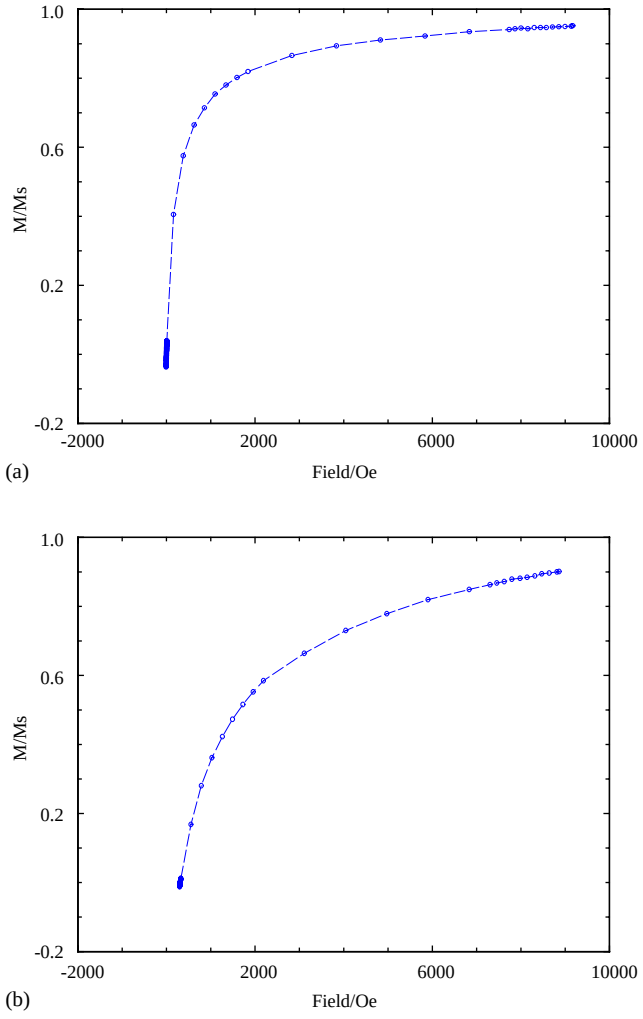

Fig. 2. Magnetisation curves for a fluid a fluid prepared from particles synthesised in the absence of dextran (a) and (b) a dextran stabilised.

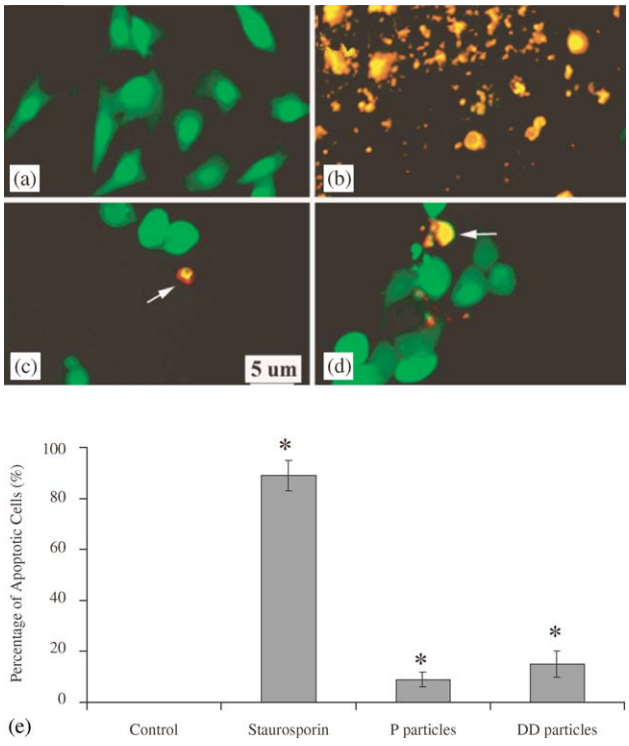

Fig. 3. Annexin V kit fluorescent staining of (a) control untreated cells, (b) staurosporin treated cells, (c) cells incubated with P particles and (d) cells incubated with DD particles. Arrows denote possible apoptotic cells. The percentage of the total number of cells that were apoptotic were counted and expressed graphically (e).

microscope (Vickers M17) with images captured using a Hamamatsu Argus 20.

2.9. Time lapse recording for cell motility

Cells were seeded at 1×10^4 cells per ml onto 6-well tissue culture plates. Cells were permitted several hours to begin adhering to the wells, prior to setting up for video recording at 37°C during nanoparticle incubation. Recordings were then made on S-VHS via an Alrad CV-M50 CCD camera on a Zeiss Axiovert 25 microscope with phase contrast objectives ($\times 10$ magnification used). The recording were used to track five individual cells over a 24 h period, with an image captured every minute and frames transferred to a computer using NIH image. In each case the distance travelled by each cell was averaged and the resultant cell motility speeds for each cell were calculated and averaged.

3. Results

3.1. Magnetic nanoparticle size determination

The TEM image of the magnetic nanoparticles was used to determine the shape, size and uniformity of the particles (Fig. 1). The picture shows that the particles are spherical shaped and monodispersed with an approximate size distribution between 10 and 15 nm.

Fig. 2 shows the relative magnetisation curve as a function of magnetic field for P and DD nanoparticles. From the figure, no hysteresis was observed which indicates the characteristic superparamagnetic behaviour of the particles. The diameter of median log volume (D_{vm}) and size distribution was calculated using the following equations based on a log-normal volume distribution [27]:

$$D_{vm} = \{18kT/I_s^1\pi[\chi_I/3I_s : 1/H_o]^{1/2}\}^{1/3}, \quad (1)$$

$$\sigma = 1/3\{Ln[3\chi_I/I_s(1/H_o)]\}^{1/2}, \quad (2)$$

$$\sigma_{red} = \sigma/D_{vm}, \quad (3)$$

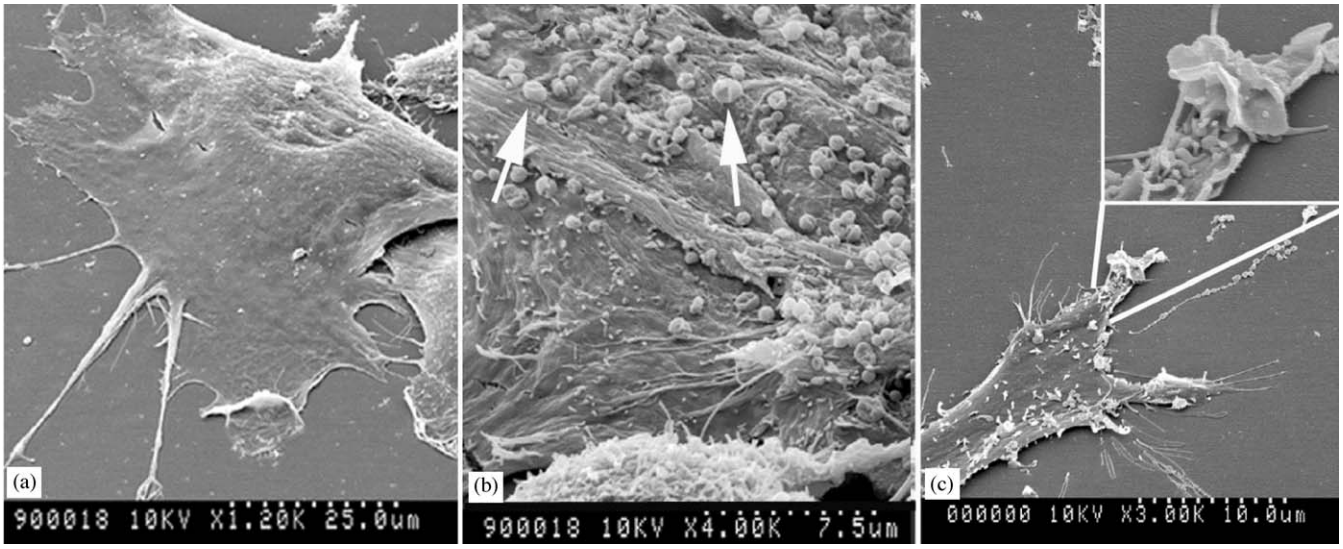

Fig. 4. SEM image of (a) control cells, (b) cells incubated with P particles and (c) cells incubated with DD particles. Arrows denote membrane disruptions.

where D_{vm} is the diameter of median log volume, χ_I the initial susceptibility; I_s the saturation magnetisation of the dispersion, I_s^1 the saturation magnetisation of the dispersed phase, T the temperature (K), k the Boltzmann constant, $1/H_o$ the intercept at the x-axis of a tangent drawn to a plot of Magnetisation versus 1/Field for high strength field values, σ the standard deviation and σ_{red} the reduced standard deviation.

The diameter of median log volume was found to be 7.8 nm with a reduced standard deviation of 0.30 for dextran (DD) particles. Similar measurements on P particles subsequently coated in oleic acid and dispersed in a carrier yielded values of D_{vm} of 9.9 nm and a reduced standard deviation of 0.46.

3.2. Cell viability/apoptosis

The annexin V kit staining is shown in Fig. 3. The control cells are all viable, with the staurosporin positive control cells mostly appearing to be in the early stages of apoptosis. Interestingly, with regards the cells exposed to P and DD nanoparticles, although the cells are mainly viable, there are several cells evident that also appear to be in the early stages of apoptosis. The percentage, through cell counts on three separate coverslips, of viable, dead and apoptotic cells were noted. Control cells were 100% viable, with P and DD exposed cells being 79% and 83% viable. The remainder percentage for P and DD nanoparticles was divided between 7% (0.4 s.d.) dead and 14% (0.75 s.d.) apoptotic, and 6% dead (0.35 s.d.) and 11% apoptotic (0.86 s.d.) respectively.

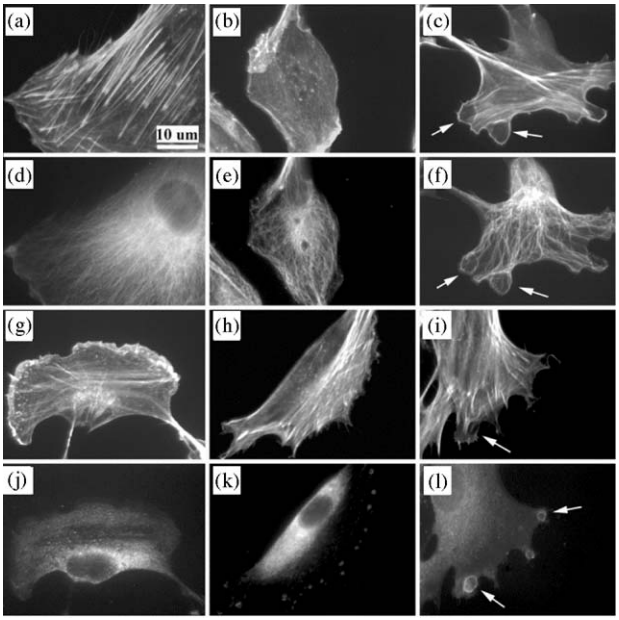

Fig. 5. Fluorescent images of F-actin and β-tubulin, or F-actin and rac, staining after 24 h culture of control cells (a, d: g, j) cells incubated with P (b, e:h, k) and cells incubated with DD (c, f: I, l) respectively. Arrows denote cell protrusions.

3.3. SEM for cell morphology

SEM observation of cell morphology for control cells demonstrated flattened, spread cells with lamellapodia (Fig. 4a). Conversely, the cells exposed to P nanoparticles appeared to cause disruptions to the cell surface membrane akin to those observed during phagocytosis [28]. Cell membranes were also disrupted in response to

DD particles, producing extremely large cell extensions similar to those observed with the P nanoparticles (Fig. 4c).

3.4. Cytoskeletal and rac images

At the 24 h particle incubation, the observed F-actin cytoskeleton was well defined with clear stress fibres for control cells, and tubulin radiating through the cytoplasm to the cell periphery (Figs. 5a and d). Cells incubated with P particles exhibited a smaller cell morphology, with actin appearing condensed and less organised (Figs. 5b and e). Meanwhile, the cells incubated with DD nanoparticles, although exhibiting clear actin fibres and tubulin radiating through the cell, both appeared to localise in large ring structures at the cell lamella (Figs. 5c and f).

Fig. 5 also shows F-actin and rac localisation, rac being involved in actin organisation at the cell lamella. Again control cells demonstrated organised actin, with ruffles evident at the cell leading edge, and background levels of rac (Figs. 5g and j). The cells incubated with P nanoparticles also demonstrated actin involvement at the cell leading edge, with rac evident through the cell and at the cell edge (Figs. 5h and k). Cells incubated with DD nanoparticles, however, exhibited similar actin ring-like structures at the cell periphery as Fig. 5c, co-localised with an increase in rac levels (Figs. 5i and l).

3.5. Fluorescent particle uptake

Figs. 6a–c show examples of fibroblasts incubated in fluorescently coated nanoparticles after 12 h culture. The P and DD fluorescent particles appear to be in clusters in the cell cytoplasm, possibly located in endocytotic vesicles. The level of fluorescence intensity due to particle uptake was measured via imageJ and expressed

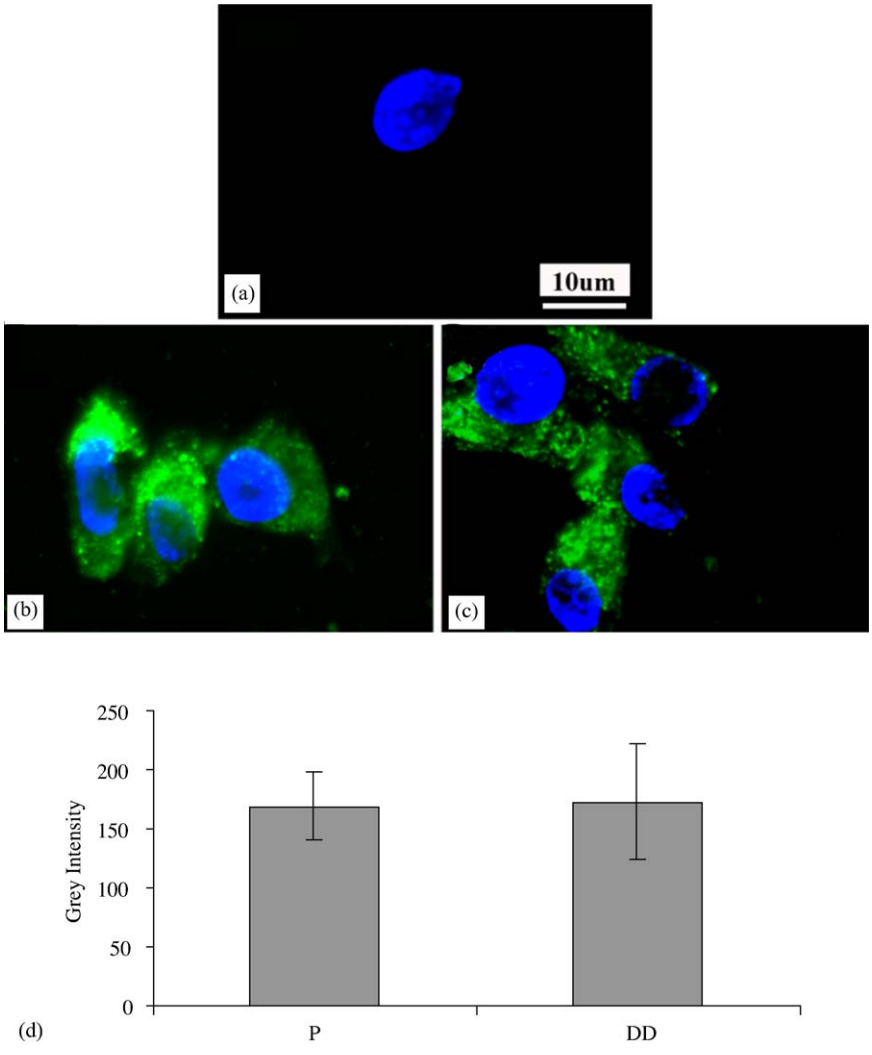

Fig. 6. Fluorescent images indicating particle uptake of (a) control cells, (b) fluorescently labeled P particles and (c) fluorescently labeled DD particles, and measurements of stain intensities, mean ± s.d. (d).

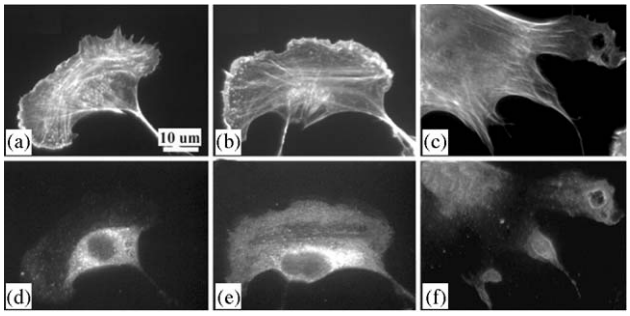

Fig. 7. Fluorescent F-actin and clathrin images for (a,d) control cells, (b,e) cells incubated with P particles and (c,f) cells incubated with DD particles, respectively.

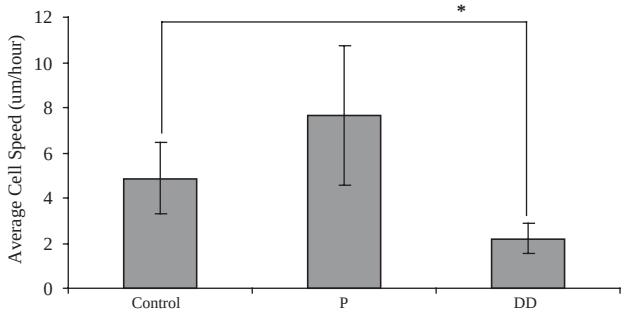

Fig. 8. Graphical representation of average cell speeds measured via time lapse microscopy (values are mean ± s.d., $p \leqslant 0.05$).

graphically in Fig. 6d. The level of uptake for both particles appears similar, with no significant difference.

3.6. Clathrin immunofluorescence

Fig. 7 indicates F-actin organisation with corresponding levels of clathrin, a protein intimately involved in the endocytosis process. Clathrin levels were shown to be elevated in cells exposed to either the P or DD nanoparticles as compared to control cells, particularly around the nucleus and cell periphery respectively (Figs. 7d–f). It was noted that the DD nanoparticles demonstrated elevated clathrin localised to the ring-like actin structures observed previously (Fig. 7c).

3.7. Cell motility

The average cell speeds were calculated from time lapse video recording of cell movement over a 24 h period and are shown in Fig. 8. The DD nanoparticles significantly inhibited cell movement while the P particles, although appearing to stimulate movement, did not induce a significant response.

4. Discussion

The magnetic nanoparticles produced were found to be in the 7–15 nm size range, well within the required size boundaries [29,30]. In addition, it was found from VSM studies and electron microscopy that the DD particles were significantly smaller than the P particles. The DD particles were precipitated from an iron salt–dextran solution and it is likely that the presence of dextran limits particles growth, leading to smaller values of particle size and standard deviation observed. Similar effects have been observed in other ferrofluids which employ oleic acid [31].

It is always important when testing a material that may be used in vivo to assess cell viability in case of material induced toxicity. While necrosis is a form of cell death resulting from direct cell damage, apoptosis is a form of cell programmed cell death where one or more cells effectively commit suicide [32]. The kit utilised in this study allowed the simultaneous visualisation of viable, necrotic and apoptotic cells in any given sample. Dextran is not noted for its cytotoxic effects directly, however it is known that upon internalisation, the dextran shell on the particles can be broken down, yielding particle chains and aggregates which may influence cell processes [33]. This, however, would not explain the cell death observed with the P nanoparticles. When collated with other results (such as the fluorescent particle uptake and the clathrin localisation), it would suggest that the P and DD nanoparticles may be inducing apoptosis due to massive particle internalisation [34,35].

The fluorescent labelling of the particles appears to have proved successful, demonstrating that the cells uptake similar levels of both P and DD nanoparticles. The possibility does remain that the cells may have merely internalised free fluorescence, but final dialysis should ensure removal of the majority of unlabelled fluorescence [27]. The mechanism of uptake for both the uncoated and dextran coated nanoparticles is most likely via fluid phase endocytosis, as reflected with the increased clathrin levels at the cell peripheries. This is further supported by a recent study which demonstrated that dextran-coated nanoparticles internalisation was non-saturable, and therefore not receptor mediated [1]. In addition, it has been reported that there are no binding centres for dextran on the plasma membrane [36,11].

Despite both the levels and methods of uptake proving similar, the cell response observed over 48-h incubation differed greatly. The first distinction was demonstrated when assessing cell morphology changes from the SEM images. Although in both cases the cell membrane was disrupted in a fashion indicative of endocytosis, the disruptions were far more pronounced in response to the DD nanoparticles. Subsequent

cytoskeletal staining showed that F-actin and β-tubulin were structurally responsible for these large membrane extensions. Interestingly, similar extensions are evident in macrophages during FcγR-mediated phagocytosis [37]. In this case, the changes in macrophage morphology observed were due to changes in actin polymerisation in response to activation of the small GTPases rac and Cdc42. The Rho family proteins are well known for their effects on the actin cytoskeleton, and it is increasingly believed that they play important roles in the trafficking of vesicles during both endocytosis and exocytosis [38]. Cdc42 is thought to drive vesicle movement through Arp2/3 complex mediated actin polymerisation at the surface of the vesicle [39], and this is similar to what is believed to happen with rac and Cdc42 stimulating actin polymerisation at the plasma membrane [40]. It certainly appears that these extensions are associated with vesicle movement as clathrin was found co-localised with the F-actin.

Rac has also been implicated in cell motility through mediating cytoskeletal rearrangements [41,42]. It is reported that increases in rac signalling can promote cell motility [43]. Indeed, increases in rac levels were obvious in response to the DD nanoparticles, clearly localising in the actin/tubulin extensions described. This would suggest these extensions are also present in the cell leading edge and implicated in cell motility, as well as internalisation. However, on measurement of the cell motility rates these cells actually demonstrated a significant decrease when compared to control cells. Cell migration is a multistep process, involving lamellipodium extension, formation of new adhesions and tail detachment [44,45]. In the cells observed here, it would appear that the first stage (lamellipodium extension) has occurred, but the subsequent steps are inhibited. The large extensions observed in the cells appear to protrude in every case from the cell lamella, for which rac is required. This would therefore explain the increased levels of rac in this area of the cell. However, why the following migration steps appear inhibited is unknown. Further studies on other GTPases involved in latter stages of cell migration may help elucidate this [46].

5. Conclusion

Dextran-coated magnetic nanoparticles have been shown to accumulate in various types of cells after several hours incubation in culture, and are currently in preclinical and clinical use in intracellular hyperthermia treatment and MRI contrast agents. However, very little is known about the influence of the particles on cells in longer-term culture, or the mechanism of uptake. This paper has clearly shown that although fibroblasts uptake the particles as required, probably through fluid phase endocytosis, the cell behaviour is adversely affected by internalisation, with results including possible apoptosis through internalisation, aberrations in cell morphology and resultant decreases in cell motility. Such findings provide important considerations when using such preparations in vivo.

References

[1] Wilhelm C, Billotey C, Roger J, Pons JN, Bacri C, Gazeau F. Inracellular uptake of anionic superparamagnetic nanoparticles as a function o their surface coating. Biomaterials 2002;24(6):1001–11.
[2] Halavaara J, Tervahartiala P, Isoniemi H, Hockerstedt K. Efficacy of sequential use of superparamagnetic iron oxide and gadolinium in liver MR imaging. Acta Radiol 2002;43(2):180–5.
[3] Lok C. Picture perfect. Nature 2001;412:372–4.
[4] Hilger I, Fruhauf K, Andra W, Hiergeist R, Hergt R, Kaiser WA. Heating potential of iron oxides for therapeutic purposes in interventional radiology. Acad Radiol 2002;9(2):198–202.
[5] Ito A, Shinkai M, Honda H, Kobatashi T. Heat-inducible TNF-alpha gene therapy combined with hyperthermia using magnetic nanopartices as a novel tumour-targeted therapy. Cancer Gene Ther 2001;8(9):649–54.
[6] Babincova M, Sourivong P, Leszczynska D, Babinec P. Blood-specific whole-body electromagnetic hyperthermia. Med Hypoth 2000;55(6):59–460.
[7] Van Beers BE, Pringot J, Gallez B. Iron oxides as contrast agents for MRI of the liver. J Radiol 1995;76(11):991–5.
[8] Lacava LM, Lacava ZGM, Da Silva MF, Silva O, Chaves SB, Azevedo RB, Pelegrini F, Gansau C, Buske N, Sabolovic D, Morais PC. Magnetic resonance of a dextran-coated magnetic fluid intravenously administered in mice. Biophys J 2001;80:2483–6.
[9] Babes L, Denzoit B, Tanguy G, Le Jeune JJ, Jallet P. Synthesis of iron oxide nanoparticles used as MRI contrast agents: a parametric study. J Colloid Interface Sci 1999;212:474–82.
[10] Babincova M, Leszczynska D, Sourivong P, Babinec P. Selective treatment of neoplastic cells using ferritin-mediated electromagnetic hyperthermia. Med Hypoth 2000;54(3):177–9.
[11] Moore A, Marecos EM, Bogdanov A, Weissleder R. Tumoral distribution of long-circulating dextran-coated iron oxide nanoparticles in a rodent model. Radiology 2000;214:568–74.
[12] Harisinghani MG, Weissleder R, et al. Differentiation of liver hemangiomas from metastases and hepatocellular carcinomas at MR imaging enhanced with blood-pool agent code-7227. Radiology 1997;2002:687–91.
[13] Berry CC, Charles S, Wells S, Dalby MJ, Curtis ASG. The influence of transferrin stabilised magnetic nanoparticles on human dermal fibroblasts in culture. Int J Pharm 2004;269:211–25.
[14] Weissleder R, Moore A, Mahmood U, Bhorade R, Benveniste H, Chiocca EA, Basilion JP. In vivo magnetic resonance imaging of transgene expression. Nat Med 2000;6:351–5.
[15] Josephson L, Tung C-H, Moore A, Weissleder R. High-efficiency intracellular magnetic labeling with novel superparamagnetic-Tat peptide conjugates. Bioconjugate Chem 1999;10:186–91.
[16] Yeh TC, Zhang W, Ildstad ST, Ho C. Intracellular labelling of T-cells with superparamagnetic contrast agents. Magn Reson Med 1993;30:617–25.
[17] Schafer DA. Coupling actin dynamics and membrane dynamics during endocytosis. Curr Opin Cell Biol 2002;14:76–81.
[18] Moore A, Weissleder R, Bogdanov A. Uptake of dexxtran-coated monocrystaline iron oxides in tumor cells and macrophages. J Magn Reson Imaging 1997;7:1140–5.

[19] Schulze E, Ferrucci JT, Poss K, Lapointe L, Bogdanova A, Weissleder R. Cellular uptake and trafficking of a prototypical magnetic iron oxide label in vitro. Invest. Radiol 1995;30:604–10.
[20] Bulte JWM, Duncan ID, Frank JA. In vivo tracking of magnetically labeled cells following transplantation. J Cerebral Blood Flow Metab 2002;22(8):899–907.
[21] Reimers GW, Khalafalla SE. US Bureau of Mines Tech Rep 1972; 59.
[22] Molday RS, Mackenzie D. Immunospecific ferromagnetic iron-dextran reagents for the labeling and magnetic separation of cells. J Immunol Methods 1982;52:353–67.
[23] Martin SJ, Reutelingsperger CP, MaGahon AJ, Kader JA, van Schie RC, La Face DM, Green DR. Early redistribution of plasma membrane phosphatidylserine is a general feature of apoptosis regardless of the initiating stimulus: inhibition by overexpression of Bcl-2. J Exp Med 1995;185(5):1545–56.
[24] Cande C, Cohen I, Daugas E, Ravagnan L, Larochette N, Zamzami N, Kroemer G. Apoptosis-inducing factor (AIF): a novel caspase-independent death effector released from mitochondria. Biochimie 2002;84(2–3):215–22.
[25] Nicotera P, Leist M, Ferrando-May E. Intracellular ATP, a switch in the decision between apoptosis and necrosis. Toxicol Lett 1998;28(102–103):139–42.
[26] Michell BB, Shiigi SM. Selected methods in cellular immunology. San Francisco: WH Freeman and Company; 1980.
[27] Granqvist CG, Buhrman RH. Ultrafine metal particles. J Appl Phys 1976;47:2200–19.
[28] Morrissette N, Gold E, Aderem A. The macrophage - a cell for all seasons. Trends Cell Biol 1999;9:199–201.
[29] Wang YX, Hussain SM, Krestin GP. Superparamagnetic iron oxide contrast agents: physicochemical characteristics and applications in MR imaging. Eur Radiol 2001;11:2319–31.
[30] Bonnemain B. Superparamagnetic agents in magnetic resonance imaging: physiochemical characteristics and clinical applications—a review. J Drug Target 1998;6:167–74.
[31] Davis KJ, Wells S, Charles SW. J Magn Magn Mater 1993;122:24.
[32] Ueda N, Shah SV. Apoptosis. J Lab Clin Med 1994;124(2): 169–77.
[33] Jordan A, Wust P, Scholz R, Tesche B, Fahling H, Mitrovics T, Vogl T, Cervos-Navarro J, Felix R. Cellular uptake of magnetic fluid particles and their effects on human carcinoma cells exposed to AC magnetic fields in vitro. Int J Hyperthermia 1996; 12(6):705–22.
[34] Huang CM, Wu YT, Chen ST. Targeting delivery of paclitaxel into tumour cells via somatostatin receptor endocytosis. Chem Biol 2000;7(7):453–61.
[35] Pioletti DP, Takei H, Kwon SY, wood D, Sung KL. The cytoxic effect of titanium particles phagocytosed by osteoblasts. J Biomed Mater Res 1999;46(3):399–407.
[36] Hacker U, Albrecht R, Maniak M. Fluid-phase uptake by macropinocytosis in *Dictyostelium*. J Cell Sci 1997;110:105–12.
[37] Caron E, Hall A. Identification of two distinct mechanisms of phagocytosis controlled by different Rho GTPases. Science 1998;282(5394):1717–21.
[38] Ridley AJ. Rho proteins: linking signaling with membrane trafficking. Traffic 2001;2:303–10.
[39] Stamnes M. Regulating the actin cytoskeleton during vesicular transport. Curr Opin Cell Biol 2002;14(4):428–33.
[40] Pollard TD, Borisy GG. Cellular motility driven by assembly and disassembly of actin filaments. Cell. 2003;112(4):453–65.
[41] Kjoller L, Hall A. Rac mediates cytoskeletal rearrangements and increased cell motility induced by urokinase-type plasminogen activator receptor binding to vitronectin. J Cell Biol 2001; 152:1145–57.
[42] Ridley AJ. Rho family proteins: coordinating cell response. Trends Cell Biol 2001;11:471–7.
[43] Price LS, Collard JG. Regulation of the cytoskeleton by Rho-family GTPases: implications for tumour cell invasion. Semin Cancer Biol 2001;11(2):167–73.
[44] Ridley AJ. Rho GTPases and cell migration. J Cell Biol 2001;114:2713–22.
[45] Mitchison T, Cramer LP. Actin based cell motility and cell locomotion. Cell 1996;84:371–9.
[46] Wittmann T, Water-Storer CM. Cell motility: can Rho GTPass and microtubules point the way. J Cell Sci 2001;114: 3795–803.